Article:
Yang, J-YT, Hsu, T-C, Tan, E et al. (2022) Sedimentary processes dominate nitrous oxide production and emission in the hypoxic zone off the Changjiang River estuary. Science of The Total Environment, 827. 154042. ISSN: 0048-9697

https://doi.org/10.1016/j.scitotenv.2022.154042

Sedimentary processes dominate nitrous oxide production and emission in the hypoxic zone off the Changjiang River estuary

Jin-Yu Terence Yang [a], Ting-Chang Hsu [b], Ehui Tan [c], Kitack Lee [d], Michael D. Krom [e,f], Sijing Kang [a], Minhan Dai [a], Silver Sung-Yun Hsiao [g], Xiuli Yan [h], Wenbin Zou [a], Li Tian [a], Shuh-Ji Kao [a,c,*]

[a] State Key Laboratory of Marine Environmental Science, College of Ocean and Earth Sciences, Xiamen University, Xiamen 361102, China

[b] School of Urban and Environmental Sciences, Huaiyin Normal University, Huaiyin 223300, China

[c] State Key Laboratory of Marine Resource Utilization in South China Sea, Hainan University, Haikou 570228, China

[d] Division of Environment and Engineering, Pohang University of Science and Technology, Pohang, Republic of Korea

[e] School of Earth and Environment, University of Leeds, Leeds LS2 9JT, UK

[f] Morris Kahn Marine Station, Department of Marine Biology, University of Haifa, Haifa 3498838, Israel

[g] Institute of Astronomy and Astrophysics, Academia Sinica, Taipei, Taiwan

[h] Institute of Marine Science and Guangdong Provincial Key Laboratory of Marine Biotechnology, College of Science, Shantou University, Shantou 515063, China

*** Corresponding authors:**

Dr. Shuh-Ji Kao, Email: sjkao@xmu.edu.cn

Abstract

Coastal oceans, known as the major nitrous oxide (N_2O) source to the atmosphere, are increasingly subject to eutrophication and concurrent near-bottom hypoxia. The natural nitrogen cycle is likely to be altered markedly in hypoxic coastal oceans. However, the processes responsible for N_2O production and emission remain elusive because of lacking field rate measurements simultaneously conducted in the water column and sediment. Here, we quantified N_2O production rates using a ^{15}N-labeled technique in the water-column and surface sediments off the Changjiang (Yangtze) River estuary, the largest hypoxic zone in the Pacific margins. Our results showed that the estuarine surface sediments were the major source for N_2O production, accounting for approximately 90% of the total water-column accumulation and consequent efflux of N_2O in the hypoxic zone, whereas the water-column nitrification and denitrification combined only contributed <10%. More importantly, the coupling of nitrification and denitrification at the presence of abundant supply and remineralization of labile organic matter was the main driver of the N_2O release from the sediment-water interface in this region. This study highlights the dominant role of benthic processes occurring at the sediment-water interface controlling the coastal N_2O budget, as the anthropogenic eutrophication and hypoxia are expanding in coastal oceans.

Keywords: coupled nitrification-denitrification; denitrification; nitrification; ^{15}N-labeled techniques; N_2O production rate; sediment-water interface

1. Introduction

Nitrous oxide (N_2O) is a powerful greenhouse gas that is ~300 times more potent in warming potential than CO_2 and is known to destroy the stratospheric ozone (Ravishankara et al., 2009), which contributes to global warming by altering radiative forcing. The concentration of atmospheric N_2O has increased by 20% during Anthropocene, largely as a result of human activities (Davidson, 2009). Identifying the dominant processes that contribute to N_2O production and the environmental factors that affect N_2O production is thus critical, but it remains poorly characterized (Bange et al., 2019; Kuypers et al., 2018; Prosser et al., 2020).

The marine ecosystem is the second largest source of atmospheric N_2O (Seitzinger et al., 2000). N_2O is known to be produced by nitrification and denitrification, two microbially-mediated pathways, which extensively occur in the water column and sediments of marine environments. Under the oxygenated condition, N_2O is produced as a by-product via ammonium oxidation (i.e., the first step of nitrification). The N_2O production rates via nitrification are elevated as oxygen level decreases (Ji et al., 2015; Löscher et al., 2012). By contrast, denitrification (i.e., the stepwise reduction of nitrate or nitrite to N_2), occurring in the suboxic/anoxic environments, forms N_2O as an intermediate product. Because of the O_2 inhibition of N_2O reduction to N_2, the hypoxic condition could be especially conducive to promoting the N_2O production via denitrification (Bourbonnais et al., 2017; Ji et al., 2015). Hence, the N_2O production via nitrification and denitrification are sensitive to ambient oxygen levels.

Among various marine environments, diverse processes in coastal oceans including estuaries and near-shore regions complicate marine nitrogen cycle. These regions are identified as hotspots for N_2O production, accounting for up to 60% of the global oceanic N_2O emissions (Bange et al., 1996). Coastal oceans are subject to severe human perturbation

for decades. The riverine nutrient loads have more than doubled over the last century due to anthropogenic inputs (Beusen et al., 2016; Lee et al., 2011), leading to global expansion of hypoxic zones in estuaries and near-shore regions (Breitburg et al., 2018). The eutrophication and seasonal hypoxia have accelerated, particularly in some large river-dominated ocean margins (RiOMars) in the vicinity of populated continents (Rabouille et al., 2008). In these large RiOMars, the input of excess nitrogenous nutrients and resultant hypoxia are altering the natural nitrogen cycling, and subsequently, the production and emission of N_2O (Seitzinger and Kroeze, 1998). For instance, the N_2O emission off the Pearl River estuary (severely perturbed by anthropogenic activities) is comparable in magnitude (1.67×10^9 g $year^{-1}$) with the total amount from 19 European inner estuaries (Lin et al., 2016). Field studies in the hypoxic RiOMars are thus crucial to validate the modeled marine N_2O fluxes and evaluate its potential evolution in response to the ongoing changes of the oceans (Codispoti, 2010; Landolfi et al., 2017; Tan et al., 2020). However, previous studies on the pathways of N_2O production are conducted in either the water column or the sediments, simultaneous measurements of N_2O production in the water column and sediments are limited.

Compared to commonly used methods of natural stable isotopes and inhibitors, the ^{15}N-labeled techniques have advantages in quantifying the rates of N-cycling processes in aquatic environments with dynamic N pools (Groffman et al., 2006). Moreover, the ^{15}N-labeled approaches have additional potentials in understanding and explaining complex N-cycling processes in complicated estuarine environments (Marchant et al., 2016).

In this study we carried out shipboard ^{15}N-labeled incubations to measure N_2O production rates via various pathways in the water column and sediments during summer off the Changjiang (Yangtze) River (CJR) estuary on the East China Sea (ECS) inner shelf, which is the largest seasonal hypoxic RiOMars in the Pacific Ocean. The surrounding waters off the CJR estuary are generally oversaturated in N_2O and thus found to release N_2O to the

atmosphere. The sea-to-air N_2O fluxes are significantly higher during late spring and summer when hypoxia occurs on the inner shelf, accounting for more than 90% of annual fluxes in this region (Chen et al., 2021). In addition, the bottom-water hypoxia is assumed to enhance the N_2O emission in this region (Wang et al., 2016b). Therefore, the aim of the present study was to gain insights into the major pathways of N_2O production and their regulators in the hypoxic zone adjacent to the CJR estuary and improve our understanding on the present and future role of such coastal systems in budgeting global atmospheric N_2O.

2. Methods

2.1. Study area

The CJR is the third largest river in the world with freshwater dischange as high as 9.2 $\times 10^{11}$ m^3 $year^{-1}$. Inputs of anthropogenic nutrients have increased steadily over decades, most of which are delivered into the coastal waters of the ECS (Dai et al., 2011; Kim et al., 2011; Yan et al., 2003). The present annual load of dissolved inorganic nitrogen (DIN) is eight times higher than that observed in 1960s, leading to frequent events of serious eutrophication and harmful algal bloom off the CJR estuary (Chai et al., 2009). Accompanying the elevated nutrient load, summer hypoxia occurs more frequently in the bottom waters due to strong stratification of water column and decomposition of organic matter (Wang et al., 2016a). The hypoxic area (DO < 62–94 μmol L^{-1}) off the CJR estuary has been increasing, extending up to more than 20,000 km^2 during the early 2000s, and this region has become one of the largest low-oxygen zones in global coastal waters (Chen et al., 2007).

2.2. Sample collection and chemical analysis

120 The cruise was conducted using the R/V *Runjiang I* on August 15–24, 2011 on the ECS
121 inner shelf off the CJR and Qiantang River (QTR) estuaries (Fig. 1). Water samples for the
122 analyses of dissolved oxygen (DO), N_2O and nutrients were collected using 12 L Niskin
123 bottles attached to a conductivity-temperature-depth (CTD, SBE 911 SeaBird) rosette
124 sampler. DO and nutrients were analyzed aboard, while samples for N_2O were poisoned with
125 100 μL saturated $HgCl_2$ solution and kept at 4°C until shore-based analysis.
126 DO concentrations were analyzed using the Winkler method. Ammonium was
127 determined by the indophenol blue spectrophotometric method, and nitrite and nitrate were
128 measured using the Autoanalyzer III system (Hsiao et al., 2014). The detection limits for
129 ammonium, nitrite and nitrate were 0.16, 0.02 and 0.07 μmol L^{-1}, respectively (Zhang et al.,
130 2001). Water-column N_2O concentrations were analyzed by a purge and trap system (Tekmar
131 Velocity XPT) coupled with a gas chromatograph (see details in Text S1; Lin et al., 2016).
132 The detection limit and precision of N_2O measurement were 30 ppb and < ±5%, respectively.
133 Based on the geographical setting and surface-water salinity (Fig. 1 and 2a), the
134 sampling sites were classified as the river-mouth (sites Y0–Y0e and N1–N5 with salinity
135 lower than 20), the inner-plume (sites in the trapezoid with salinity of 20–29), and the high-
136 salinity (sites Y4–Y7, Y12 and Y19 with salinity higher than 29) zones. Physical and
137 chemical parameters measured at these sites provided the hydrographical background of the
138 study area, which showed the extent of the hypoxic zone and the influences of riverine inputs
139 over the study period (Fig. 2). N_2O production rates were determined in the inner-plume
140 zone, which was the previously reported hypoxic zone.
141 In the inner-plume zone (i.e., the hypoxic zone) the ^{15}N-labeled incubation
142 experiments for the water and sediment samples were performed at twelve and nine stations,
143 respectively (Fig. 1). Water samples were collected at 2–5 layers from the surface to the
144 bottom and filled in 100 mL narrow-necked gas-tight glass bottles (Wheaton). Each bottle

was flushed twice and overflowed before being filled without any headspace to avoid air contamination, and then sealed with a butyl rubber stopper and an open-top aluminum crimp cap (CNW) (Lin et al., 2016). Twenty sample-filled bottles were recovered at each depth and stored at room temperature for less than 1 h before the ^{15}N-labeled experiments.

Sediment samples were taken using a Soutar-type box corer and then subsampled by the Plexiglas tubes (30 cm long, 4.5 cm diameter) on deck. All intact sediment cores were carefully adjusted to 22 cm long with 8 cm of overlying water. These cores were subsequently sealed with rubber stoppers, and immediately equilibrated in a barrel filled with bottom waters at 25°C overnight (Tan et al., 2019). Four intact sediment cores were kept in the dark at in situ temperature for 4 h. The total oxygen utilization (TOU) of the surface sediments was determined based on the DO changes in the overlying waters (Rysgaard et al., 2004). Approximately 0.1 g of dry surface sediment was acidified with 1 mL of 1 N HCl to remove inorganic carbon. The decarbonated samples were used to measure sedimentary organic carbon content (SOC%) by Carbon Analyzer (Horiba EMIA).

2.3. Measurements of N_2O production rates via nitrification and denitrification in the water column

To determine the N_2O production rates via the water-column nitrification (rN_2O-WCN), ^{15}N-labeled NH_4Cl (98 ^{15}N atom%, Sigma-Aldrich) were added to ten sample-filled bottles using 100 μL gas-tight syringes (Hamilton, USA) to reach final concentrations of 10 μmol ^{15}N L^{-1} inside. It is worth noting that, because of very low N_2O yield via nitrification, higher concentrations of ^{15}N-labeled NH_4^+ relative to the ambient NH_4^+ concentrations were added to ensure the produced N_2O measurable (Punshon and Moore, 2004).

These bottles were gently shaken to ensure the tracer well mixed. Two bottles were immediately fixed by adding 0.2 mL of saturated $HgCl_2$ as initials. The remaining eight

bottles were incubated in a water bath at in situ temperature in the dark, and duplicate samples were stopped by adding $HgCl_2$ at 6-h intervals over a 24-hour incubation. After incubation, all the fixed samples were kept upside down for future isotopic analysis. The same procedure and condition were used to determine the N_2O production rates via the water-column denitrification (rN_2O-WCD), except for adding ^{15}N-labeled $NaNO_3$ (98 ^{15}N atom%, Sigma-Aldrich) to reach final concentrations of 10 μmol ^{15}N L^{-1} in the bottles.

Isotopic signals of N_2O in the bottles were measured by isotope ratio mass spectrometer (IRMS) mounted with a modified dilution pre-concentration system that allowed measurements of the isotopic signals of N_2 at the same time (Hsu and Kao, 2013). The rN_2O-WCN and rN_2O-WCD at each sampling depth were quantified based on the increases of $^{45}N_2O$ and $^{46}N_2O$ over time ($\Delta^{45}N_2O$ and $\Delta^{46}N_2O$):

$$rN_2O\text{-WCN or } rN_2O\text{-WCD} = (\Delta^{45}N_2O + 2 \times \Delta^{46}N_2O) / (F \times V) \quad (1)$$

where F represents the ^{15}N fraction in the bottle at the beginning of incubation, V is the bottle volume. The detection limit of the N_2O production rate was 0.005 nmol L^{-1} d^{-1}.

2.4. Measurement of N_2O production rates from intact sediment cores

Twenty intact sediment cores at each site were used to perform a concentration-series experiment to determine the rates of in situ N_2O production from sediments (Hsu and Kao, 2013; Trimmer et al., 2006). Briefly, $Na^{15}NO_3$ (98 ^{15}N atom%, Sigma-Aldrich) were added into the in-site overlying waters of intact sediment cores to reach a concentration gradient in range of 10–100 μmol ^{15}N L^{-1} with an increasing interval of 10 μmol ^{15}N L^{-1} following Tan et al. (2019). The overlying water of intact sediment core was then carefully stirred by a small stir bar ensuring that the sediment surface remained undisturbed throughout the pre-incubation period. The pre-incubation time was 15–30 mins to achieve a stable ^{15}N-labeled signal reaching the sedimentary denitrification zone (Hsu and Kao, 2013). All cores were

sealed and incubated in the dark at in situ temperature. Ten intact sediment cores were sacrificed immediately after the pre-incubation as initials. The remaining cores were stopped after 3 h incubation. Because the produced amounts of N_2O and N_2 in the surface sediments were small during the incubation, we suggested that they were overwhelmingly dissolved in the pore water and the overlying water.

Generally, sedimentary nitrogen loss occurs within the top 2 cm of sediments off the CJR estuary, especially in summer (e.g., Wei et al., 2022). To stop the incubation, the top 2 cm of sediments were mixed gently with the overlying waters using a plexiglass rod with a 2 cm mark (Dalsgaard et al., 2000). Subsequently, 4 mL of mixed slurry was pipetted into a 12-mL gas-tight vial (Exetainer) filling with 100 μL of formaldehyde solution (38% w/v) and a glass bead (5 mm diameter) for mixing. After capping all vials, the vial headspace was purged with helium for 1 min to remove the remaining air inside for eliminating its possible effect on the measurement of the produced N_2 (Tan et al., 2019). All vials were kept upside down at room temperature before isotopic measurements. Isotopic signals of N_2O ($^{44}N_2O$, $^{45}N_2O$, $^{46}N_2O$) and N_2 ($^{28}N_2$, $^{29}N_2$, $^{30}N_2$) in the vials were measured using the same IRMS system as the water-sample measurements.

According to the revised ^{15}N isotope pairing technique (IPT) proposed by Hsu and Kao (2013), the N_2O production rates via canonical denitrification (pN_2O-den) and coupled nitrification-denitrification (pN_2O-cnd) in sediments were quantified based on the production rates of $^{45}N_2O$, $^{46}N_2O$, $^{29}N_2$ and $^{30}N_2$ (P_{45}, P_{46}, P_{29} and P_{30}) and the genuine ratio between $^{14}NO_3^-$ and $^{15}NO_3^-$ undergoing nitrate reduction (r_{14}), using the following equations:

$$pN_2O\text{-den} = 2 \times r_{14} \times (r_{14} + 1) \times P_{46} \quad (2)$$

$$pN_2O\text{-cnd} = 2 \times r_{14} \times (P_{45} - P_{46} \times 2 \times r_{14}). \quad (3)$$

$$pN_2O\text{-SED} = pN_2O\text{-den} + pN_2O\text{-cnd} = 2 \times r_{14} \times (P_{45} + (1 - r_{14}) \times P_{46}) \quad (4)$$

where pN_2O-SED denotes the gross sedimentary N_2O production rate. The r_{14} is related to the ^{15}N proportion in the total produced N_2O pool (qN_2O) or that in the total produced N_2 pool (qN_2) (Trimmer et al., 2006). Theoretically if the canonical denitrification is the sole process to reduce $^{15}NO_3^-$ in sediments, the qN_2O would be equal to the qN_2. In other words, the slope of qN_2O vs. qN_2 ($S_{N2O/N2}$) would be 1. Anammox could form hybrid N_2 with one nitrogen atom from unlabeled nitrogen pool and the other from the ^{15}N-labeled pool, while the coupled nitrification-denitrification could form hybrid N_2O. Therefore, when anammox or the coupled nitrification-denitrification occurring in sediments contributes substantially to N_2 or N_2O production, the $S_{N2O/N2}$ is expected to be larger or lower than one. In this case, the r_{14} may be biased at the presence of anammox or the coupled nitrification-denitrification. We thus estimated the relative contribution of the pN_2O-cnd to the pN_2O-SED (R_{cnd}, %), using the following equation that is related to the $S_{N2O/N2}$ (Trimmer et al., 2006):

$$R_{cnd} = (2 - 2 \times S_{N2O/N2}) / (2 - S_{N2O/N2}) \quad (5).$$

By combining the equations 2–5, the pN_2O-den, pN_2O-cnd, pN_2O-SED and r_{14} can be calculated, respectively. In addition, we also calculated the N_2 production rates in the surface sediments (pN_2-SED) using the following equation (Hsu and Kao, 2013):

$$pN_2\text{-SED} = 2 \times (r_{14} + 1) \times r_{14} \times P_{30} \quad (6).$$

2.5. Sea-to-air N_2O flux

Sea-to-air N_2O flux (F_{N2O}, μmol m^{-2} d^{-1}) was estimated using equation 6:

$$F_{N2O} = k \times (C_{obs} - C_{eq}) = k \times \Delta N_2O \quad (7)$$

where C_{obs} is the observed concentration of dissolved N_2O in seawater; and C_{eq} is the dissolved N_2O concentration at in situ temperature and salinity that is equilibrated with its atmospheric concentration (Weiss and Price, 1980). The global mean atmospheric N_2O concentration of 324.2 ppb was used for the calculation in this study. The calculated C_{eq}

values in the surface waters of the sampling sites ranged from 6.5 to 7.2 nmol L^{-1} (Text S2 and Table S1). ΔN_2O means the discrepancy between C_{obs} and C_{eq}, indicating the excess N_2O. k (cm h^{-1}) denotes the gas transfer velocity, which is expressed as a function of the wind speed and the Schmidt Number (Sc) derived from temperature. In this study, k was calculated using the following equation given by Wanninkhof (1992):

$$k = 0.39 \times u_{10}^2 \times (Sc / 660)^{-0.5} \quad (8)$$

where u_{10} is the wind speed at the height of 10 m, with an average value of 5.2±2.6 m s^{-1} observed during the entire cruise. In addition, N_2O saturation (R_{N2O}, %) was estimated using equation 8:

$$R_{N2O} = (C_{obs} / C_{eq}) \times 100 \quad (9)$$

2.6. Statistical analysis

Correlations of concentrations and production rates of N_2O with environmental factors were tested using Pearson's correlation. A one-way analysis of variance (ANOVA) was used to determine the significant differences in N_2O production rates via water-column nitrification and denitrification. The statistical analyses were performed using SPSS at a 0.05 significance level unless otherwise indicated.

3. Results

3.1. Hydrochemistry in the water column

Both temperature and salinity in the surface and bottom waters showed zonal distributions across the study area (Fig. 2 and Fig. S1). The lowest salinity (~0.2) and highest temperature (> 29°C) were found in the surface water at site Y0 off the CJR mouth. The low-salinity waters observed in the study area were primarily related to the CJR plume, because the CJR discharge during the study period was more than 80 times higher than the QTR

discharge (MWR of China, 2012). As a result of mixing with ambient open ocean waters, salinity increased dramatically up to 34.4 in the bottom water at site Y4. The temperature-salinity (T-S) properties in the study area were controlled by three water masses, the CJR freshwater, the northward Nearshore Kuroshio Branch Current (NKBC) and the westward East China Sea Surface Water (ECSSW) (Fig. 1 and 3a; Yan et al., 2017).

Concentrations of dissolved inorganic nitrogen (DIN, in which nitrate comprised more than 98%) in the surface and bottom waters were higher than 130 μmol L^{-1} near the CJR and QTR mouths but decreased to < 4 μmol L^{-1} at the offshore sites (Fig. 2). Our measurements showed that the distribution of DIN was largely controlled by the mixing of the three water masses indicated above (Fig. 3b). The freshwater with high level of DIN was diluted by the N-depleted ESCSW and low-NO_3^- NKBC. However, the surface DIN at some high-salinity sites showed non-conservative behavior, as evidenced by some data points deviated from the conservative mixing lines of the three water masses (Fig. 3b). This was likely due to nitrate assimilation by phytoplankton (Yan et al., 2017). In addition, NH_4^+ concentrations were generally low in the study area, ranging from undetectable to 2.0 μmol L^{-1} (Fig. S1).

DO concentrations were high in the river-mouth (151–194 μmol L^{-1}) and high-salinity zones (140–249 μmol L^{-1}), but low (62–183 μmol L^{-1}) in the inner-plume zone (Fig. 2e and f), indicating that the DO distribution was not mainly regulated by the water mixing. Low levels of DO down to ~62.0 μmol L^{-1} (i.e., hypoxia) were detected in both the surface and bottom waters of the inner-plume zone. Such low concentrations of DO during summer were consistent to the previous report in this region (Zhu et al., 2011).

3.2. Surface sediment characteristics

The SOC% varied from 0.19% to 0.64%, with the lowest values at the deeper sites Y8 and Y4 where the bottom-water DO concentrations were low (81–108 μmol L^{-1}; Table 1).

The TOU in the surface sediments ranged from 11.0 to 53.6 mmol m^{-2} d^{-1} (Table 1). The lowest TOU was found at the shallower sites N0 and Y1 near the river-mouth zone. At site Y8 near the hypoxic center, we found the highest TOU in the surface sediments.

3.3. Distribution of N_2O concentration and its sea-to-air flux in the hypoxic zone

N_2O concentrations at most sites were high below the surface waters (Fig. 2 and S2). This vertical pattern is commonly observed in this region (Wang et al., 2016b; Zhang et al., 2010), and in other coastal waters (e.g., the northern South China Sea and Bay of Bengal) (Han et al., 2013; Rao et al., 2013). Spatially, N_2O concentrations showed similar distributions in the surface and bottom waters. A substantially higher N_2O concentration, up to 17.8 nmol L^{-1}, was observed near the CJR mouth. The values decreased markedly to less than 10.0 nmol L^{-1} away from the river mouth at site Y0e. The N_2O concentrations off the QTR mouth, ranging from 7.0 to 9.0 nmol L^{-1}, were considerably lower (Fig. 2g). In the inner- and high-salinity zones we observed a patch of elevated N_2O concentrations below the surface waters (Fig. 2g and h), which was spatially associated with the hypoxic core. According to the mixing lines of three water masses we found that the N_2O was mainly accumulated in the intermediate and bottom waters, suggesting its non-conservative nature (Fig. 3c).

In the hypoxic zone the average concentration of surface N_2O was 9.4±1.6 nmol L^{-1}, higher than the average surface-water N_2O concentration in equilibrium with the atmosphere (6.4±0.2 nmol L^{-1}). The surface N_2O saturation ranged from 111% to 175% with an average value of 144±21% (Table 2). An average bottom-water N_2O concentration was 10.6±2.2 nmol L^{-1} and was also oversaturated (111–194%, Table 2). The sea-to-air N_2O fluxes in the hypoxic zone were 3.6–15.0 μmol m^{-2} d^{-1} with a mean value of 8.9±4.1 μmol m^{-2} d^{-1} during the study period (Fig. 4a and Table 2). We also found that the sea-to-air N_2O flux was highest

in the vicinity of the low-oxygen center. Our values were in good agreement with the previous observations made off the CJR estuary during summer (Chen et al., 2021). A hotspot for N_2O release is commonly present during summer in the hypoxic zone off the CJR estuary.

3.4. Rates of N_2O production in the water column

In the hypoxic zone off the CJR estuary, the rN_2O-WCD rates were found to be extremely low, ranging from 0 to 0.11 nmol L^{-1} d^{-1} with an average of 0.01±0.02 nmol L^{-1} d^{-1} (Table S2). The rN_2O-WCD rates were below the detection limit at most sites. The highest rN_2O-WCD rate was observed in the bottom water at site Y9a with the lowest DO concentration. By contrast, the rN_2O-WCN rates varied between 0–0.24 nmol L^{-1} d^{-1} with a mean value of 0.04±0.05 nmol L^{-1} d^{-1} (Table S2). The rN_2O-WCN rates were generally higher below the surface waters. Similarly, the maximum rN_2O-WCN rate was found in the bottom water at site Y8 close to the hypoxic center.

With the rN_2O-WCD and rN_2O-WCN at the sampling depth, we calculated the depth-integrated N_2O production via water-column denitrification and nitrification (pN_2O-WCD and pN_2O-WCN), respectively (Table 2). The pN_2O-WCD rates were generally at very low levels (0–1.37 μmol m^{-2} d^{-1}) and spatially homogeneous, whereas the pN_2O-WCN rates ranged between 0.11–4.74 μmol m^{-2} d^{-1} with higher values found at the low-oxygen center (Fig. 4). The average pN_2O-WCD and pN_2O-WCN rates in the hypoxic zone were estimated to be 0.26±0.50 μmol m^{-2} d^{-1} and 1.39±1.48 μmol m^{-2} d^{-1}, respectively (Table 2). In summary, the N_2O production rates via the water-column nitrification were considerably higher than those via the water-column denitrification (ANOVA, $p < 0.05$).

3.5. Rates of N_2O and N_2 production in the surface sediments

From the concentration-series experiments of the intact sediment cores the $S_{N2O/N2}$ values were found to vary between 0.25 and 0.89 across the study area (Table 2), indicating that the qN_2O were lower than the qN_2 at all sampling sites. The potential anammox activities were not determined from the anoxic slurry incubation experiments (Texts S3 and S4; Fig. S3). Similarly, only a minor contribution of anammox to total sedimentary nitrogen removal was observed off the CJR estuary (Liu et al., 2019). These findings suggested that the qN_2 in the study area were not significantly diluted by the effect of the anammox process. By contrast, the qN_2O in the surface sediments were diluted by the hybrid N_2O production via the coupled nitrification-denitrification that incorporated unlabeled nitrogen from NH_4^+ or organics (see below). The R_{cnd} was in the range of 19.9–85.9% (average of 58.6±22.7%) with values greater than 50% at seven of nine sites (Table 2).

The pN_2O-den ranged from 1.6 to 9.0 μmol m^{-2} d^{-1} with the lowest rate found at site Y1 and the highest rate at site Y3. The pN_2O-cnd varied by over an order of magnitude, from 2.0 to 31.0 μmol m^{-2} d^{-1}. Unlike to the pN_2O-den showing a patchy distribution, the pN_2O-cnd increased seaward from the vicinity of the river mouth to the low-oxygen zone. The highest pN_2O-cnd was found at site Y8 where was close to the hypoxic center and the TOU in the surface sediments was highest. By contrast, the lowest pN_2O-cnd was found at sites Y1 and N0 near the river mouth where the bottom-water DO was high and the sedimentary TOU was relatively low (Tables 1 and 2). In summary, the pN_2O-SED ranged from 4.4 to 36.0 μmol m^{-2} d^{-1} (mean of 15.0±9.4 μmol m^{-2} d^{-1}), showing a distribution pattern similar to the pN_2O-cnd (Fig. 4).

The pN_2-SED ranged from 0.3 to 6.3 mmol m^{-2} d^{-1} off the CJR estuary, with higher rates near the river mouth and lower rates close to the hypoxic center (Fig. 4g and Table S3). The distribution of the pN_2-SED was roughly contrasted with that of the pN_2O-SED. The highest N_2O:N_2 production ratio (11.80%) in sediments was found at site Y8 where the pN_2-

SED was lowest and the pN_2O-SED was highest (Fig. 4h). The sedimentary N_2O:N_2 production ratios at other sites in the hypoxic zone off the CJR estuary were relatively low and varied within a narrow range (0.09–1.18%; Table S3).

4. Discussion

This is, to our knowledge, the first report of simultaneous measurements of the N_2O production rates in the water column and sediments in the hypoxic zone off the CJR estuary. The results allow us to understand how the environmental factors affect the water-column and sedimentary N_2O production and offer clear evidence for the main driver of N_2O production and emission in this hypoxic zone.

4.1. Key environmental factors affecting the water-column N_2O production

The rN_2O-WCD rates were undetectable at most sites (Fig. 4b), indicating that the water-column denitrification was suppressed in this hypoxic zone over the study period. This is likely because the water-column denitrification can only efficiently produce N_2O at the oxic-anoxic interface (DO < 5 μmol L^{-1}; Codispoti et al., 2001). Although the extent of hypoxia off the CJR estuary has been increasing since 1950s, the bottom-water DO minimum varies between 10 and 60 μmol L^{-1} all the time (Zhu et al., 2011). Hence, the contribution of the water-column denitrification to the water-column N_2O production is very limited off the CJR estuary.

The rN_2O-WCN rates were significantly higher than the rN_2O-WCD rates in this hypoxic zone ($n = 42$, $p < 0.01$), suggesting that nitrifying microorganisms were more active relative to denitrifiers. This finding was supported by the evidence of microbial communities and geochemical indicators observed during this cruise. For example, Zhang et al. (2014) reported that the copy numbers of the ammonia monooxygenase gene (including bacterial and archaeal *amoA*) were significantly higher than those of the dissimilatory nitrite reductase

394 gene *nirS* in this region. Dual isotope measurements revealed that the nitrate dynamics in this
395 summer was predominated by the water-column nitrification, rather than the water-column
396 denitrification (Yan et al., 2017). On the other hand, increasing rates of the water-column
397 N_2O production were strongly associated with decreasing DO concentrations in the hypoxic
398 zone (Fig. S4a). Neither DIN nor particle concentrations in the water column were
399 significantly correlated with the water-column N_2O production rates (Fig. S5). Therefore,
400 these results suggested that ambient DO concentration was the important factor regulating the
401 N_2O formation in the water column and that low-oxygen condition enhanced the N_2O
402 production.
403 Notably, the total water-column N_2O production rate of 1.7±1.6 μmol m^{-2} d^{-1} in the
404 hypoxic zone off the CJR estuary is at the low limit of the reported N_2O production rates in
405 other estuarine waters (Murray et al., 2015). Considering that the water-column nitrification
406 rates were 100–3200 nmol L^{-1} d^{-1} during this cruise (Hsiao et al., 2014), we found that the
407 average N_2O yield via nitrification was only 0.007%. This value is lower than that found in
408 other coastal waters (0.01–0.42%; de Wilde and de Bie, 2000; Punshon and Moore, 2004).
409 The optimum condition for nitrifiers to produce N_2O is expected to be 10–30 μmol O_2 L^{-1} or
410 O_2 saturation of 2–15% (de Bie et al., 2002; Punshon and Moore, 2004). We thus speculated
411 that the nitrifiers were not efficiently conducting N_2O production, since the water-column DO
412 concentrations were not low enough over the study period. Caution is needed on the declining
413 oxygen in estuaries and coastal waters (Breitburg et al., 2018), which may result in an
414 enhancement of the water-column N_2O production.
415
416 4.2. Key environmental factors affecting the sedimentary N_2O production
417 The incubation results showed that the surface sediments were a net N_2O source in the
418 hypoxic zone off the CJR estuary. The measured in situ sedimentary N_2O production rates in

419 this study (4.4–36.0 μmol m^{-2} d^{-1}) fall into the reported ranges of the sedimentary N_2O fluxes
420 (2.4–240 μmol m^{-2} d^{-1}) observed in other eutrophic RiOMars (Murray et al., 2015; Sun et al.,
421 2014; Tan et al., 2019). Previous study has reported that the potential sedimentary N_2O
422 production rates near the river-mouth zone are higher than those in the hypoxic zone based on
423 the slurry experiments (Lin et al., 2017). However, the in situ sedimentary N_2O production
424 rates are comparable between the two zones off the CJR estuary based on the intact sediment
425 experiments (0.1–36.0 μmol m^{-2} d^{-1} observed near the river-mouth zone; Chen et al., 2021;
426 Chen et al., 2022; Wang et al., 2007; Zhang et al., 2010). Thus, the sediment N_2O release in
427 the hypoxic zone may play an important role in contributing to the regional N_2O budget.
428 The sedimentary N_2O production was predominated by coupled nitrification-
429 denitrification especially at sites with relatively low DO concentrations (Fig. 5). As a result,
430 the pN_2O-cnd were closely correlated with the pN_2O-SED and bottom-water DO (Table 3).
431 The importance of nitrification-related pathway to sedimentary N_2O production may be
432 related to the abundance of autotrophic and heterotrophic nitrifiers that simultaneously
433 consume organic carbon and ammonium in the surface sediments off the CJR estuary (Jin et
434 al., 2017; Zheng et al., 2014). We also noted that the pN_2O-den and pN_2-SED had no
435 significant relationship with bottom-water NO_3^-, suggesting that the major substrate for
436 denitrification did not come from the nitrate diffused from the overlying waters into
437 sediments. Instead, the nitrification-derived nitrate may primarily fuel the sedimentary
438 denitrification. A tight interaction between denitrification and nitrification generally occurs at
439 the oxic-anoxic interface of estuarine sediments and is conducive to sedimentary N_2O
440 production (Liu et al., 2019; Tan et al., 2019). The pN_2O-cnd were positively correlated with
441 the TOU in the surface sediments and the R_{cnd} were negatively correlated with the SOC%
442 (Table 3). In addition, the positive relationship was observed between the sedimentary
443 N_2O:N_2 production ratio and the TOU. Remineralization of organic matter in sediments

444 provides the substrate (i.e., NH_4^+) for the nitrification and creates anaerobic condition for
445 denitrification. Recent studies have indicated that the quality of sediment organic matter
446 determines the N_2O fluxes in coastal sediments, showing that marine organic matter
447 stimulates N_2O production (Chen et al., 2022; Lin et al., 2017). During this cruise particulate
448 organic matter was mainly of marine source produced in situ, and its remineralization
449 dominantly contributed to oxygen consumption in this region (Wang et al., 2016a). Thus,
450 increasing remineralization of labile sedimentary organic matter may lead to increases in the
451 N_2O production via coupled nitrification-denitrification in the surface sediments.
452 Active nitrification occurs at the sediment-water interface, in contrast to
453 denitrification occurring in the deeper anoxic sediment layers (Hou et al., 2007; Wankel et
454 al., 2017). The N_2O produced by sedimentary nitrification would easily diffuse into the
455 overlying water and subsequently be released to the atmosphere (Meyer et al., 2008). Results
456 from this study highlight a substantial role of sedimentary nitrification in stimulating N_2O
457 production and emission in the hypoxic RiOMars.
458
459 4.3. The N_2O budget in the hypoxic zone off the Changjiang estuary
460 The hypoxic zone off the CJR estuary acted as a net source of N_2O to the atmosphere,
461 with higher fluxes in the low-oxygen center (Fig. 4a). On the other hand, the positive ΔN_2O
462 values and its inventory suggested the N_2O accumulation in the water column of the hypoxic
463 zone (Fig. S6). The ΔN_2O values were positively correlated with the apparent oxygen
464 utilization (AOU; Pearson correlation, $R^2 = 0.35$, $p < 0.001$) and negatively correlated with
465 DO (Pearson correlation, $R^2 = 0.41$, $p < 0.001$) in this region (Fig. 3d and S4b), indicating
466 that the accumulation of N_2O was enhanced under the low-oxygen condition. These findings
467 were consistent with higher rates of in situ N_2O production observed at low-oxygen sites
468 (Fig. 4).

To further evaluate the relative contributions of the water-column and sedimentary processes to the N_2O budget in the hypoxic zone, we considered that the exchange of waters in the hypoxic zone with the surrounding waters were limited over the study period. This assumption was supported by the results that strong stratification of the water column and gradual formation of subsurface hypoxia were observed over the study period (Fig. S7; Wang et al., 2016a). External pathways had limited influence on the N_2O budget in the hypoxic zone during the study period. Explicitly, the high levels of N_2O from river input were confined to the areas near the river mouth only and the N_2O concentrations rapidly decreased away from the river mouth (Fig. 2g and 3c). This finding suggested that most of N_2O in the river-mouth zone were released to the atmosphere because of the high N_2O supersaturation (up to 220%) in the water column. Thus, the N_2O production via the water-column and sedimentary processes was the major source of N_2O and the sea-to-air emission was the main sink of N_2O (Fig. 6).

In a steady state, the gross N_2O production within the system was balanced by the sum of the sea-to-air N_2O flux and the water-column N_2O accumulation taking into account the water residence time (τ). The amount of the water-column N_2O accumulation, determined by the ΔN_2O inventory, was 134.8±101.5 μmol m^{-2} (Table 2). By dividing the ΔN_2O inventory by the difference between the gross rate of the water-column and sedimentary N_2O production (16.7±9.5 μmol m^{-2} d^{-1}) and the sea-to-air N_2O flux (8.9±4.1 μmol m^{-2} d^{-1}; Table 2), the τ was calculated to be 17.3±1.5 days. The estimated τ was in agreement with a previous report of the water exchange time (~16 days) off the CJR estuary based on the water and salt budgets (Li et al., 2011), strengthening the plausibility of this estimate. Our observation showed that in the hypoxic zone off the CJR estuary the sedimentary N_2O production overwhelmingly contributed to the water-column N_2O accumulation and the N_2O emission to the atmosphere (~90%) relative to a minor contribution (<10%) from the water-

column N_2O production. As a result, the distribution of the pN_2O-SED was spatially coincident with those of the sea-to-air N_2O fluxes and the ΔN_2O inventory (Figs. 4 and S6). Taken together, our results suggest the predominant role of sedimentary processes in regulating the N_2O budget of the hypoxic RioMars.

5. Concluding remarks

Results from this study showed that the low-oxygen levels may increase the water-column and sedimentary N_2O production rates in the hypoxic zone off the CJR estuary. We concluded that the benthic processes played the major role in the accumulation of water-column N_2O and its emission to the atmosphere. Such high rates of sedimentary N_2O production were mainly supported by coupled nitrification-denitrification, which was likely related to the input and remineralization of labile sedimentary organic matter. These quantitative results provide evidence of the main mechanisms which result in the hypoxic zone of this human-perturbed margin as a significant source of N_2O.

As severe surface eutrophication and near-bottom hypoxia in the estuarine and coastal systems are predicted to increase, amounts of fresh labile organic matter deposited onto surface sediments will increase. This may lead to an increase in N_2O production from the sediment-water interface and subsequent N_2O emission to the atmosphere. Such effects could be expected in this area (Lin et al., 2017) and other renowned human-perturbed hypoxic coastal oceans, such as the Indian coast, the Gulf of Mexico and the Baltic Sea (Conley et al., 2011; Kim et al., 2013; Naqvi et al., 2000). Therefore, our study highlights that as areas of coastal hypoxia increase, it is likely that coastal sediments will result in increasing N_2O fluxes to the atmosphere and hence enhance the global greenhouse effect. This study thus has implications for decision-making that seeks to mitigate N_2O emission and its impact on climate change.

Acknowledgements

We thank Liguo Guo, Lifang Wang and Tao Huang for their assistance in the laboratory works. This work was supported by the Strategic Priority Research Program of Chinese Academy of Sciences (Grant #XDB42000000), the National Natural Science Foundation of China (Grants #41721005, #91851209, #92058204, #41730533, #41890804), the Fundamental Research Funds for the Central Universities (Grants #20720190092, #20720212005) and State Key Laboratory of Marine Resource Utilization in South China Sea (Hainan University) (Grant #MRUKF2021018). We also thank two anonymous reviewers for their constructive comments and suggestions. The data used in this study are available in the article and supporting materials.

References

Bange, H.W., Arévalo-Martínez, D.L., de la Paz, M., Farías, L., Kaiser, J., Kock, A., et al., 2019. A Harmonized Nitrous Oxide (N_2O) Ocean Observation Network for the 21st Century. Front. Mar. Sci. 6, 157. doi:10.3389/fmars.2019.00157

Bange, H.W., Rapsomanikis, S., Andreae, M.O., 1996. Nitrous oxide in coastal waters. Global Biogeochem. Cycles 10, 197-207. doi:10.1029/95GB03834

Beusen, A.H.W., Bouwman, A.F., Van Beek, L.P.H., Mogollón, J.M., Middelburg, J.J., 2016. Global riverine N and P transport to ocean increased during the 20th century despite increased retention along the aquatic continuum. Biogeosciences 13, 2441-2451. doi:10.5194/bg-13-2441-2016

Bourbonnais, A., Letscher, R.T., Bange, H.W., Échevin, V., Larkum, J., Mohn, J., et al., 2017. N_2O production and consumption from stable isotopic and concentration data in the Peruvian coastal upwelling system. Global Biogeochem. Cycles 31, 678-698. doi:10.1002/2016GB005567

Breitburg, D., Levin, L.A., Oschlies, A., Grégoire, M., Chavez, F.P., Conley, D.J., et al., 2018. Declining oxygen in the global ocean and coastal waters. Science 359, eaam7240. doi:10.1126/science.aam7240

Chai C., Yu, Z., Shen, Z., Song, X., Cao, X, Yao, Y., 2009. Nutrient characteristics in the Yangtze River Estuary and the adjacent East China Sea before and after impoundment of the Three Gorges Dam, Sci. Total Environ. 407, 4687-4695. doi:10.1016/j.scitotenv.2009.05.011

Chen, C.-C., Gong, G.-C., Shiah. F.-K., 2007. Hypoxia in the East China Sea: One of the largest coastal low-oxygen areas in the world. Mar. Environmen. Res. 64, 399-408. doi:10.1016/j.marenvres.2007.01.007

553 Chen, X., Ma, X., Gu, X., Liu, S., Song, G., Jin, H., et al., 2021. Seasonal and spatial
554 variations of N_2O distribution and emission in the East China Sea and South Yellow Sea.
555 Sci. Total Environ. 775, 145715. doi:10.1016/j.scitotenv.2021.145715
556 Chen, S., Wang, D., Yu, Z., Nie, J., Chen, J., Li, Y., et al., 2022. Quality of sediment organic
557 matter determines the intertidal N_2O response to global warming. J. Geophys. Res. -
558 Biogeosciences. doi:10.1029/2021JG006572
559 Codispoti, L.A., 2010. Interesting times for marine N_2O. Science 327, 1339-1340.
560 Codispoti, L.A., Brandes, J.A., Christensen, J.P., Devol, A.H., Naqvi, S.W.A., Paerl, H.W., et
561 al., 2001. The oceanic fixed nitrogen and nitrous oxide budgets: moving targets as we
562 enter the anthropocene? Sci. Mar. 65, 85-105. doi:10.3989/scimar.2001.65s285
563 Conley D.J., Carstensen, J., Aigars, J., Axe, P., Bonsdorff, E., Eremina, T., et al., 2011.
564 Hypoxia is increasing in the coastal zone of the Baltic Sea. Environmen. Sci. Technol. 45,
565 6777-6783. doi:10.1021/es201212r
566 Dai, Z., Du, J., Zhang, X., Su, N. and Li, J., 2011. Variation of riverine material loads and
567 environmental consequences on the Changjiang (Yangtze) Estuary in Recent Decades
568 (1955−2008). Environmen. Sci. Technol. 45, 223-227. doi:10.1021/es103026a
569 Dalsgaard, T., Nielsen, L.P., Brotas, V., Viaroli, P., Underwood, G.J.C., Nedwell, D.B., et al.,
570 2000. Protocol Handbook for NICE - Nitrogen Cycling in Estuaries: A Project under the
571 EU Research Programme : Marine Science and Technology (MAST III), National
572 Environmental Research Institute, Denmark.
573 Davidson, E.A. 2009. The contribution of manure and fertilizer nitrogen to atmospheric
574 nitrous oxide since 1860. Nat. Geosci. 2, 659-662. doi:10.1038/NGEO608
575 de Bie, M.J.M., Middelburg, J.J., Starink, M., Laanbroek, H.J., 2002. Fators controlling
576 nitrous oxide at the microbial community and estuarine scale. Mar. Ecol. Progr. Ser. 240,
577 1-9. doi:10.3354/meps240001

578 de Wilde, H.P.J., de Bie, M.J.M., 2000. Nitrous oxide in the Schelde estuary: production by
579 nitrification and emission to the atmosphere. Mar. Chem. 69, 203-216.
580 doi:10.1016/S0304-4203(99)00106-1
581 Han, Y., Zhang, G.-L., Zhao, Y.-C., Liu, S.-M., 2013. Distributions and sea-to-air fluxes of
582 nitrous oxide in the coastal and shelf waters of the northwestern South China Sea. Estuar.
583 Coast. Shelf Sci. 133, 32-44. doi:10.1016/j.ecss.2013.08.001
584 Hou, L.J., Liu, M., Xu, S.Y., Ou, D.N., Yu, J., Cheng, S.B., et al., 2007. The effects of semi-
585 lunar spring and neap tidal change on nitrification, denitrification and N_2O vertical
586 distribution in the intertidal sediments of the Yangtze estuary, China. Estuar. Coast. Shelf
587 Sci. 73, 607-616. doi:10.1016/j.ecss.2007.03.002
588 Hsiao, S.S.-Y., Hsu, T.-C., Liu, J.-W., Xie, X., Zhang, Y., Lin, J., et al., 2014. Nitrification
589 and its oxygen consumption along the turbid Chang Jiang River plume. Biogeosciences
590 11, 2083-2098. doi:10.5194/bg-11-2083-2014
591 Hsu, T.C., Kao, S.J., 2013. Technical Note: Simultaneous measurement of sedimentary N_2
592 and N_2O production and a modified ^{15}N isotope pairing technique. Biogeosciences 10,
593 7847-7862. doi:10.5194/bg-10-7847-2013
594 Ji, Q., Babbin, A.R., Jayakumar, A., Oleynik, S., Ward, B.B., 2015. Nitrous oxide production
595 by nitrification and denitrification in the Eastern Tropical South Pacific oxygen minimum
596 zone. Geophys. Res. Lett. 42, 10755-10764. doi:10.1002/2015GL066853
597 Jin, Q., Lu, J., Wu, J., Luo, Y., 2017. Simultaneous removal of organic carbon and nitrogen
598 pollutants in the Yangtze estuarine sediment: The role of heterotrophic nitrifiers. Estuar.
599 Coast. Shelf Sci. 191, 150-156. doi:10.1016/j.ecss.2017.04.019
600 Kim, I.N., Lee, K., Bange, H.W., Macdonald, A.M., 2013. Interannual variation in summer
601 N_2O concentration in the hypoxic region of the northern Gulf of Mexico, 1985–2007.
602 Biogeosciences 10, 6783-6792. doi:10.5194/bg-10-6783-2013

603 Kim, T.-W., Lee, K., Najjar, R.G., Jeong, H.-D., Jeong, H.-J., 2011. Increasing N abundance
604 in the northwestern Pacific Ocean due to atmospheric nitrogen deposition. Science 334,
605 505-509. doi:10.1126/science.1206583
606 Kuypers, M.M.M., Marchant, H.K., Kartal, B., 2018. The microbial nitrogen-cycling
607 network. Nat. Rev. Microbiol. 16, 263-276. doi:10.1038/nrmicro.2018.9
608 Landolfi, A., Somes, C.J., Koeve, W., Zamora, L.M., Oschlies, A., 2017. Oceanic nitrogen
609 cycling and N_2O flux perturbations in the Anthropocene. Global Biogeochem. Cycles 31,
610 1236-1255. doi:10.1002/2017GB005633
611 Lee, K., Chris, S., Tanhua, T., Kim, T.-W., Feely, R., Kim, H.-C., 2011. Roles of marginal
612 seas in absorbing and storing fossil fuel CO_2. Energ. Environ. Sci. 4, 1133-1146.
613 doi:10.1039/C0EE00663G
614 Lin, H., Dai, M., Kao, S.J.,Wang, L., Roberts, E., Yang, J.Y.T., et al., 2016. Spatiotemporal
615 variability of nitrous oxide in a large eutrophic estuarine system: The Pearl River Estuary,
616 China. Mar. Chem. 182, 14-24. doi:10.1016/j.marchem.2016.03.005
617 Lin, X., Liu, M., Hou, L., Gao, D., Li, X., Lu, K., et al., 2017. Nitrogen losses in sediments of
618 the East China Sea: Spatiotemporal variations, controlling factors, and environmental
619 implications. J. Geophys. Res. - Biogeosciences 122, 2699-2715.
620 doi:10.1002/2017JG004036
621 Liu, C., Hou, L., Liu, M., Zheng, Y., Yin, G., Han, P., et al., 2019. Coupling of denitrification
622 and anaerobic ammonium oxidation with nitrification in sediments of the Yangtze Estuary:
623 Importance and controlling factors. Estuar. Coastal Shelf Sci. 220, 64-72.
624 doi:10.1016/j.ecss.2019.02.043
625 Löscher, C.R., Kock, A., Könneke, M., LaRoche, J., Bange, H.W., Schmitz, R.A., 2012.
626 Production of oceanic nitrous oxide by ammonia-oxidizing archaea. Biogeosciences 9,
627 2419-2429. doi:10.5194/bg-9-2419-2012

628 Meyer, R.L., Allen, D.E., Schmidt, S., 2008. Nitrification and denitrification as sources of
629 sediment nitrous oxide production: A microsensor approach. Mar. Chem. 110, 68-76.
630 doi:10.1016/j.marchem.2008.02.004
631 Ministry of Water Resources of the People's Republic of China (MWR of China), 2012.
632 River sediment bulletin of China (2011), China Water & Power Press, Beijing.
633 Murray, R.H., Erler, D.V., Eyre, B.D., 2015. Nitrous oxide fluxes in estuarine environments:
634 response to global change. Global Change Biol. 21, 3219-3245. doi:10.1111/gcb.12923
635 Naqvi, S.W.A., Jayakumar, D.A., Narvekar, P.V., Naik, H., Sarma, V.V.S.S., D'Souza, W., et
636 al., 2000. Increased marine production of N_2O due to intensifying anoxia on the Indian
637 continental shelf. Nature 408, 346-349. doi:10.1038/35042551
638 Prosser, J.I., Hink, L., Gubry-Rangin, C., Nicol, G.W., 2019. Nitrous oxide production by
639 ammonia oxidizers: Physiological diversity, niche differentiation and potential mitigation
640 strategies. Global Change Biol. 26, 103-118. doi:10.1111/gcb.14877
641 Punshon, S., Moore, R., 2004. Nitrous oxide production and consumption in a euthophic
642 coastal embayment. Mar. Chem. 91, 37-51. doi: 10.1016/j.marchem.2004.04.003
643 Rabouille, C., Conley, D.J., Dai, M.H., Cai, W.J., Chen, C.T.A., Lansard, B., et al., 2008.
644 Comparison of hypoxia among four river-dominated ocean margins: The Changjiang
645 (Yangtze), Mississippi, Pearl, and Rhône rivers. Continent. Shelf Res. 28, 1527-1537.
646 doi:10.1016/j.csr.2008.01.020
647 Rao, G.D., Rao, V.D., Sarma, V.V.S.S., 2013. Distribution and air–sea exchange of nitrous
648 oxide in the coastal Bay of Bengal during peak discharge period (southwest monsoon).
649 Mar. Chem. 155, 1-9. doi:10.1016/j.marchem.2013.04.014
650 Ravishankara, A.R., Daniel, J.S., Portmann, R.W., 2009. Nitrous Oxide (N_2O): The dominant
651 ozone-depleting substance emitted in the 21st century. Science 326, 123-125.
652 doi:10.1126/science.1176985

653 Rysgaard, S., Glud, R.N., Risgaard-Petersen, N., Dalsgaard, T., 2004. Denitrification and
654 anammox activity in Arctic marine sediments. Limnol. Oceanogr. 49, 1493-1502.
655 doi:10.4319/lo.2004.49.5.1493
656 Seitzinger, S.P., Kroeze, C., 1998. Global distribution of nitrous oxide production and N
657 inputs in freshwater and coastal marine ecosystems. Global Biogeochem. Cycles 12, 93-
658 113. doi:10.1029/97GB03657
659 Seitzinger, S.P., Kroeze, C., Styles, R.V., 2000. Global distribution of N_2O emissions from
660 aquatic systems: natural emissions and anthropogenic effects. Chemosphere - Global
661 Change Sci. 2, 267-279. doi:10.1016/S1465-9972(00)00015-5
662 Sun, Z., Wang, L., Mou, X., Jiang, H., Sun, W., 2014. Spatial and temporal variations of
663 nitrous oxide flux between coastal marsh and the atmosphere in the Yellow River estuary
664 of China. Environmen. Sci. Pollut. Res. 21, 419-433. doi:10.1007/s11356-013-1885-5
665 Tan, E., Zou, W., Jiang, X., Wan, X., Hsu, T.-C., Zheng, Z., et al., 2019. Organic matter
666 decomposition sustains sedimentary nitrogen loss in the Pearl River Estuary, China. Sci.
667 Total Environ. 648, 508-517. doi:10.1016/j.scitotenv.2018.08.109
668 Tan, E., Zou, W., Zheng, Z., Yan, X., Du, M., Hsu, T.-C., et al., 2020. Warming stimulates
669 sediment denitrification at the expense of anaerobic ammonium oxidation. Nat. Clim.
670 Change 10, 349–355. doi:10.1038/s41558-020-0723-2
671 Trimmer, M., Risgaard-Petersen, N., Nicholls, J.C., Engström, P., 2006. Direct measurement
672 of anaerobic ammonium oxidation (anammox) and denitrification in intact sediment cores.
673 Mar. Ecol. Progr. Ser. 326, 37-47. doi:10.3354/meps326037
674 Wang, D., Chen, Z., Wang, J., Xu, S., Yang, H., Chen, H., et al., 2007. Summer-time
675 denitrification and nitrous oxide exchange in the intertidal zone of the Yangtze Estuary.
676 Estuar. Coast. Shelf Sci. 73, 43-53. doi:10.1016/j.ecss.2006.11.002

677 Wang, H., Dai, M., Liu, J., Kao, S.-J., Zhang, C., Cai, W.-J., et al., 2016a. Eutrophication-
678 driven hypoxia in the East China Sea off the Changjiang Estuary. Environmen. Sci.
679 Technol. 50, 2255-2263. doi:10.1021/acs.est.5b06211
680 Wang, L., Zhang, G., Zhu, Z., Li, J., Liu, S., Ye, W., et al., 2016b. Distribution and sea-to-air
681 flux of nitrous oxide in the East China Sea during the summer of 2013. Continent. Shelf
682 Res. 123, 99-110. doi:10.1016/j.csr.2016.05.001
683 Wankel, S.D., Ziebis, W., Buchwald, C., Charoenpong, C., de Beer, D., Dentinger, J., et al.,
684 2017. Evidence for fungal and chemodenitrification based N_2O flux from nitrogen
685 impacted coastal sediments. Nat. Commun. 8, 15595. doi:10.1038/ncomms15595
686 Wanninkhof, R., 1992. Relationship between wind speed and gas exchange over the ocean. J.
687 Geophys. Res. - Oceans 97, 7373-7382. doi:10.1029/92JC00188
688 Wei, L., Cai, P., Shi, X., Cai, W.-J., Liu, W., Hong, Q., et al., 2022. Winter mixing
689 accelerates decomposition of sedimentary organic carbon in seasonally hypoxic coastal
690 seas. Geochim. Cosmochim. Acta 317, 457-471. doi:10.1016/j.gca.2021.11.003
691 Weiss, R.F., Price, B.A., 1980. Nitrous oxide solubility in water and seawater. Mar. Chem. 8,
692 347-359. doi:10.1016/0304-4203(80)90024-9
693 Yan, X., Xu, M.N., Wan, X.S., Yang, J.-Y.T., Trull, T.W., Dai, M., et al., 2017. Dual isotope
694 measurements reveal zoning of nitrate processing in the summer Changjiang (Yangtze)
695 River plume. Geophys. Res. Lett. 44, 12289-12297. doi:10.1002/2017GL075951
696 Yan, W., Zhang, S. Sun, P., Seitzinger, S.P., 2003. How do nitrogen inputs to the Changjiang
697 basin impact the Changjiang River nitrate: A temporal analysis for 1968–1997. Global
698 Biogeochem. Cycles 17, 1091. doi:10.1029.2002GB002029
699 Zhang, G.L., Zhang, J., Liu, S.M., Ren, J.L., Zhao, Y.C., 2010. Nitrous oxide in the
700 Changjiang (Yangtze River) Estuary and its adjacent marine area: Riverine input,

sediment release and atmospheric fluxes. Biogeosciences 7, 3505-3516. doi:10.5194/bg-7-3505-2010

Zhang, J.-Z., Wanninkhof, R., Lee, K., 2001. Enhanced new production observed from the diurnal cycle of nitrate in an oligotrophic anticyclonic eddy. Geophys. Res. Lett. 28, 1579-1582. doi:10.1029/2000GL012065

Zhang, Y., Xie, X., Jiao, N., Hsiao, S.S.Y., Kao, S.J., 2014. Diversity and distribution of *amoA*-type nitrifying and *nirS*-type denitrifying microbial communities in the Yangtze River estuary. Biogeosciences 11, 2131-2145. doi:10.5194/bg-11-2131-2014

Zheng, Y., Hou, L., Newell, S., Liu, M., Zhou, J., Zhao, H., et al., 2014. Community dynamics and activity of ammonia-oxidizing prokaryotes in intertidal sediments of the Yangtze Estuary. Appl. Environmen Microbiol. 80, 408-419. doi:10.1128/AEM.03035-13

Zhu, Z.Y., Zhang, J., Wu, Y., Zhang, Y.Y., Lin, J., Liu, S.M., 2011. Hypoxia off the Changjiang (Yangtze River) Estuary: Oxygen depletion and organic matter decomposition. Mar. Chem. 125, 108-116. doi:10.1016/j.marchem.2011.03.005

715 **Table 1.** Sampling information of sediment in the hypoxic zone off the Changjiang River estuary. Salinity, concentrations of dissolved oxygen
716 (DO) and nitrate (NO_3^-) in the bottom waters at each site are also shown. SOC% and TOU indicate sedimentary organic carbon content and total
717 oxygen utilization, respectively.

718

Station	Sampling date	Bottom Depth (m)	Salinity	Bottom DO (μmol L^{-1})	Bottom NO_3^- (μmol L^{-1})	SOC%	TOU (mmol m^{-2} d^{-1})
N0	August 18	26	26.8	164	40.4	0.50	11.0
Y1	August 17	12	23.1	183	52.4	0.41	11.4
Y2	August 17	20	29.3	143	28.7	0.52	15.1
Y3	August 19	23	32.2	133	24.5	0.64	26.3
Y4	August 20	56	34.4	108	12.8	0.19	25.9
Y8	August 21	63	33.8	81	16.3	0.25	53.6
Y10	August 22	48	32.8	81	15.1	0.50	16.3
Y17	August 16	23	30.5	167	11.9	0.57	19.4
Y18	August 22	42	28.7	88	19.6	0.56	31.8

Table 2. Concentrations (C_{N2O}, nmol L^{-1}) and saturations of N_2O (R_{N2O}, %) in the surface and bottom waters, the sea-to-air N_2O flux (F_{N2O}, μmol m^{-2} d^{-1}) and the water-column inventory of excess N_2O ($I_{\Delta N2O}$, μmol m^{-2}) in the hypoxic zone off the Changjiang River estuary. We compare the N_2O production rates (μmol m^{-2} d^{-1}) via the water-column nitrification (pN_2O-WCN), denitrification (pN_2O-WCD) and sedimentary processes (pN_2O-SED) at sampling sites. The slope of the ^{15}N proportion in the total produced N_2O pool vs. that in total produced N_2 pool ($S_{N2O/N2}$) and the relative contribution of N_2O production via coupled nitrification-denitrification in sediment to the pN_2O-SED (R_{cnd}, %) are also shown.

Station	Surface waters		Bottom waters		F_{N2O}	$I_{\Delta N2O}$	pN_2O-WCD*	pN_2O-WCN	pN_2O-SED*	$S_{N2O/N2}$*	R_{cnd}*
	C_{N2O}	R_{N2O}	C_{N2O}	R_{N2O}							
N0	9.0	135	7.4	111	7.1	29.0	0.02	0.60	10.01	0.89	19.9
Y1	10.6	156	10.5	157	11.5	45.6	0.01	0.24	4.38	0.52	64.5
Y2	8.0	118	8.3	121	3.6	25.0	0.09	0.11	9.27	0.54	62.8
Y3	10.4	156	13.7	194	11.2	112.0	0.02	0.60	12.02	0.85	25.5
Y4	7.2	111	9.6	127	2.2	91.0	0.25	0.34	16.63	0.30	82.1
Y8	12.5	175	12.2	165	15.0	305.1	0.11	4.74	36.03	0.25	85.9
Y9	10.0	153	10.7	148	10.7	118.4	0.02	2.36	n.s.	n.s.	n.s.
Y9a	10.2	146	13.2	178	9.1	285.9	1.28	3.54	n.s.	n.s.	n.s.
Y10	12.0	173	13.7	188	14.4	282.8	1.37	1.86	18.58	0.52	64.6
Y11	7.7	118	8.3	118	3.6	111.9	n.d.	0.23	n.s.	n.s.	n.s.
Y17	9.3	140	9.1	131	7.9	63.4	0.01	0.65	8.55	0.64	52.8
Y18	10.0	151	11.0	150	10.1	148.0	n.d.	1.42	19.64	0.47	69.2
Mean±SD	9.4±1.6	144±21	10.6±2.2	149±28	8.9±4.1	134.8±101.5	0.26±0.50	1.39±1.48	15.01±9.36	0.55±0.22	58.6±22.7

* n.d. and n.s. denote not detected and not sampled, respectively.

Table 3. Correlation matrix of variables in the bottom water and surface sediment. Note that only statistically significant correlations between variables are shown. DO: dissolved oxygen; TOU: total oxygen utilization in surface sediment; SOC%: sedimentary organic carbon content; pN_2O-SED: total sedimentary N_2O production rate; pN_2O-den: N_2O production rate via sedimentary denitrification; pN_2O-cnd: N_2O production rate via coupled nitrification-denitrification in sediment; R_{cnd}: the relative contribution of the pN_2O-cnd to the pN_2O-SED; pN_2-SED: total sedimentary N_2 production rate; N_2O:N_2: sedimentary N_2O:N_2 production ratio.

Variable	DO	Salinity	NO_3^-	TOU	SOC%	pN_2O-SED	pN_2O-den	pN_2O-cnd	R_{cnd}	pN_2-SED
DO										
Salinity	–0.71*									
NO_3^-	0.67*	–0.88**								
TOU	–0.67*	–	–							
SOC%	–	–	–	–						
pN_2O-SED	–0.84**	–	–	0.91**	–					
pN_2O-den	–	–	–	–	–	–				
pN_2O-cnd	–0.79*	–	–	0.89**	–	0.97**	–			
R_{cnd}	–	–	–	–	–0.69*	–	–	0.73*		
pN_2-SED	–	–	–	–	–	–	–	–	–	
N_2O:N_2	–	–	–	0.85**	–	0.87**	–	0.88**	–	–0.69*

* Correlation is significant at the 0.05 level
** Correlation is significant at 0.01 level

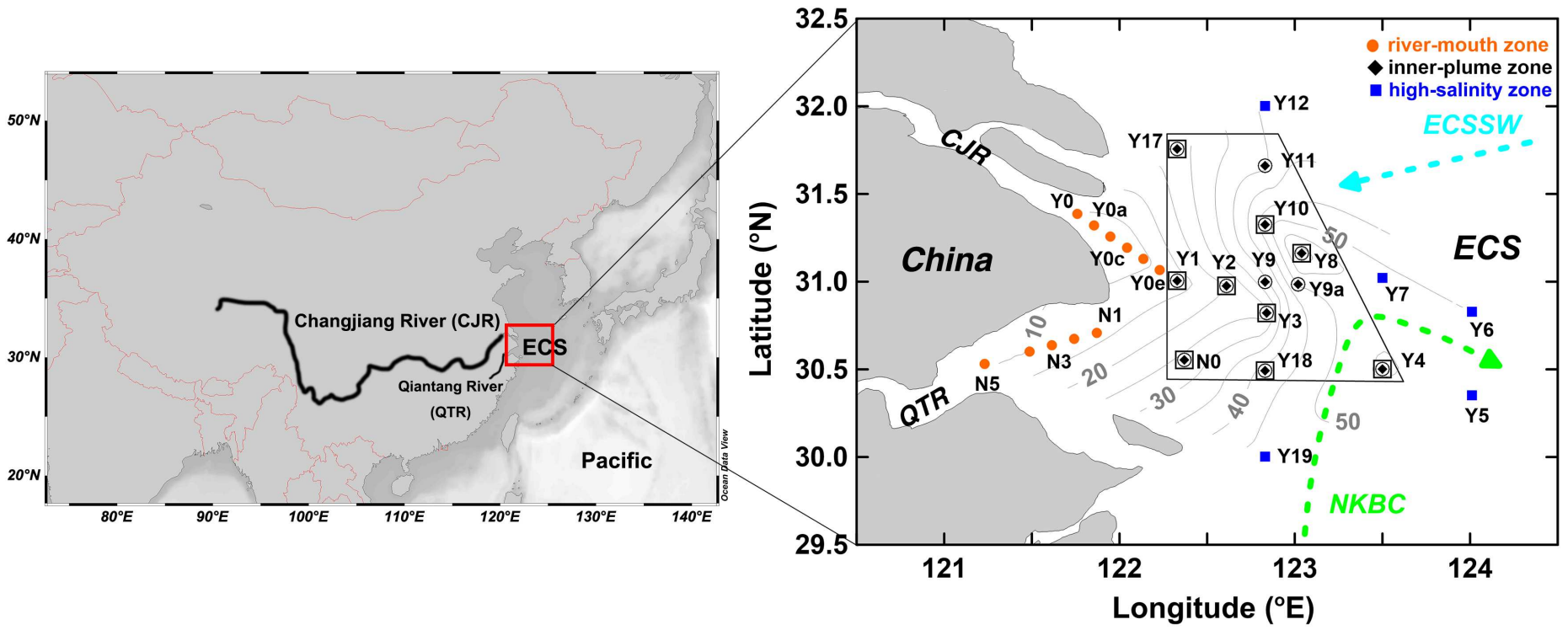

733

734 **Fig. 1.** Map of sampling sites off the Changjiang River (CJR) and Qiantang River (QTR) estuaries on the East China Sea (ECS) shelf. Water

735 samples were collected at all sites. The ^{15}N-labeled incubations for N_2O production via the water-column (◈) and sedimentary (▣) processes

736 were conducted in the inner-plume zone, which was the previously reported hypoxic zone in this region (shown in the trapezoid). The green and

737 light blue dashed arrows show the pathways of the NKBC and ECSSW from the outer shelf, respectively. The contours indicate the water depth

738 in the study area.

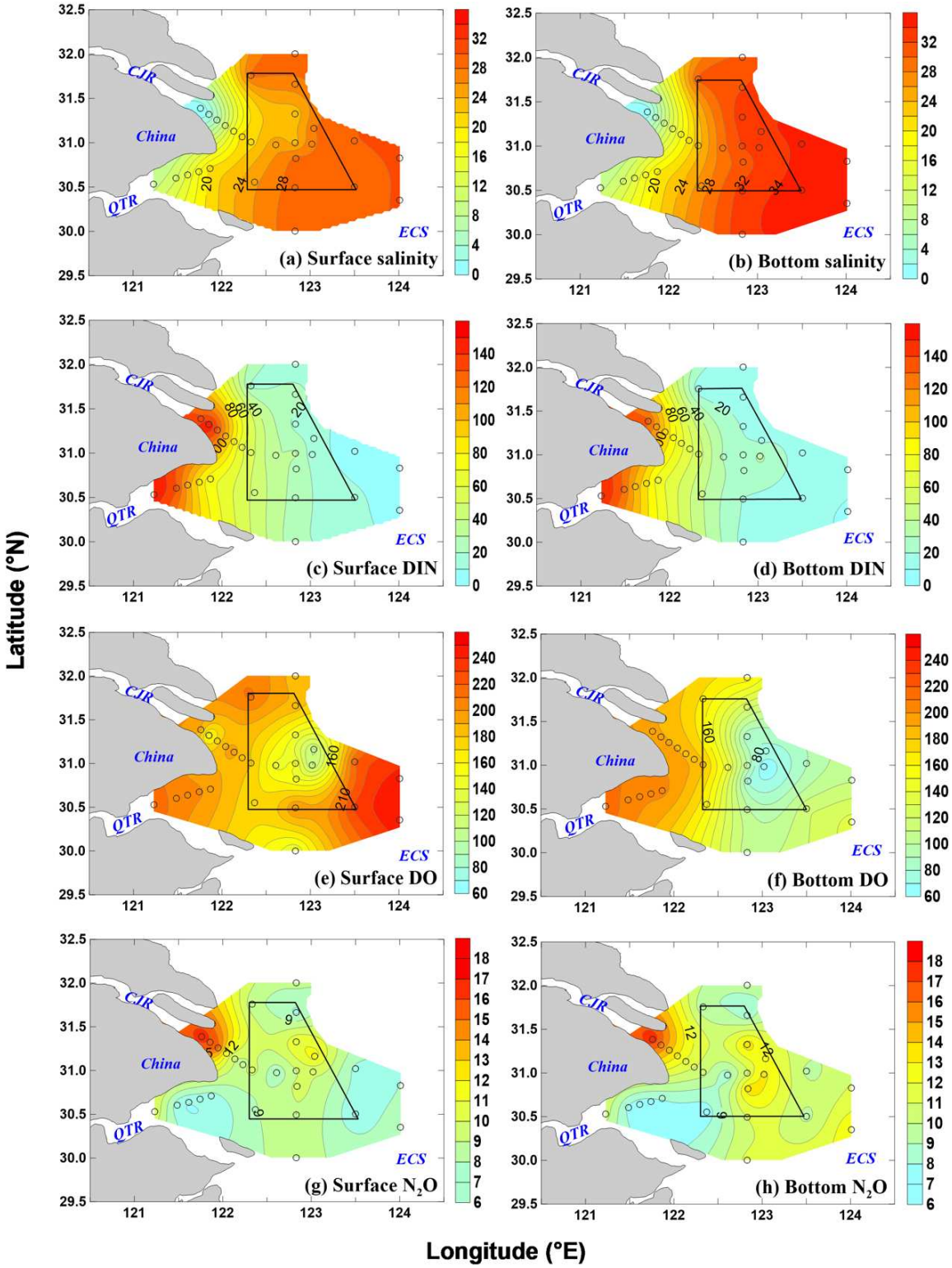

739

740 **Fig. 2.** Spatial distribution of salinity (a and b), concentrations of DIN (c and d, μmol L^{-1}),

741 DO (e and f, μmol L^{-1}), and N_2O (g and h, nmol L^{-1}) in the surface and bottom waters.

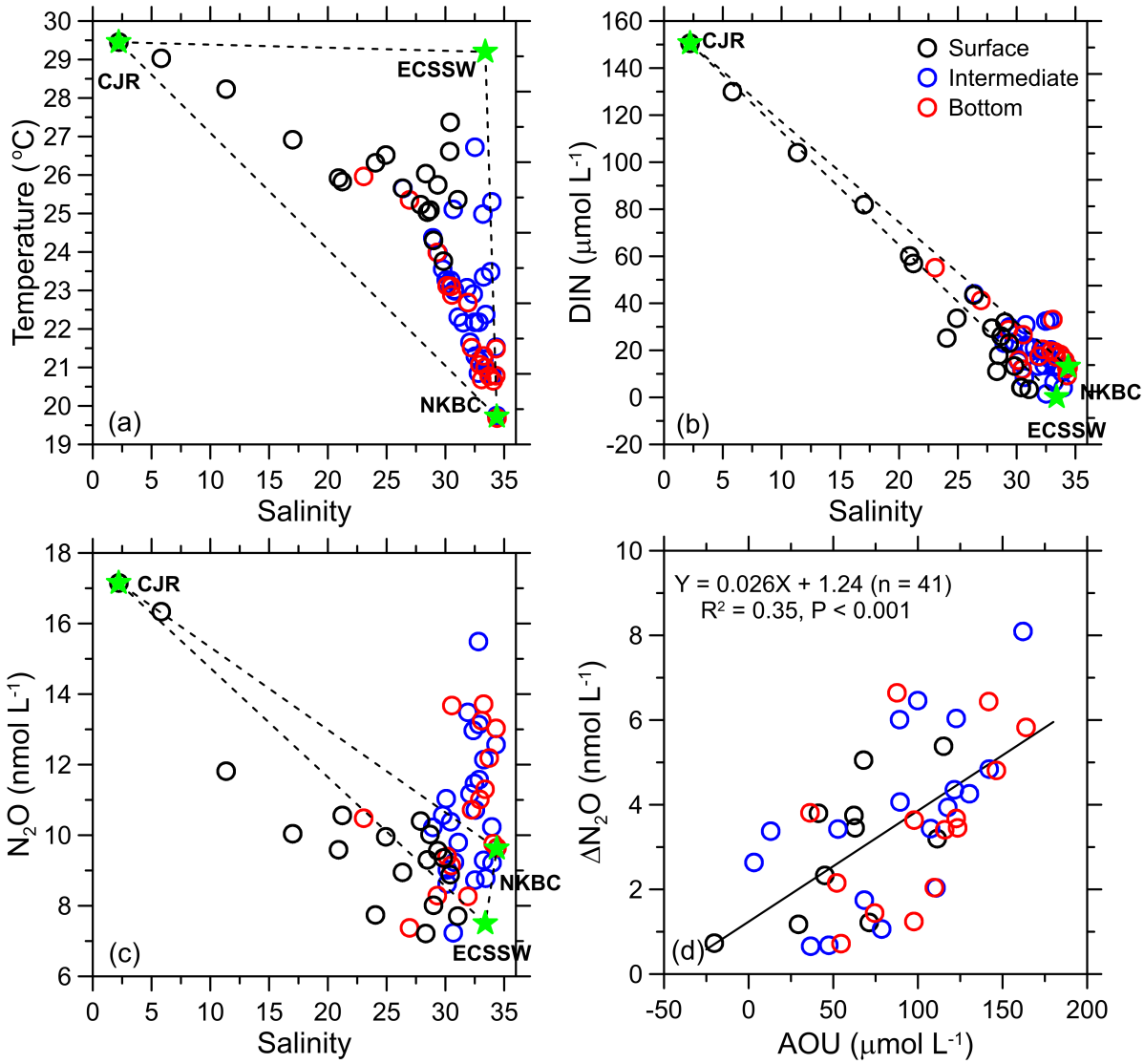

742

743 **Fig. 3.** Scatter plots of salinity vs. temperature (a), DIN (b), N_2O (c), and AOU vs. ΔN_2O (d)

744 in the study area. Relevant endmembers of three water masses are shown as green stars in a–c

745 (see text). The dotted lines in (a–c) represent conservative mixing curves of different water

746 masses. Note that only data from the hypoxic zone are shown in (d).

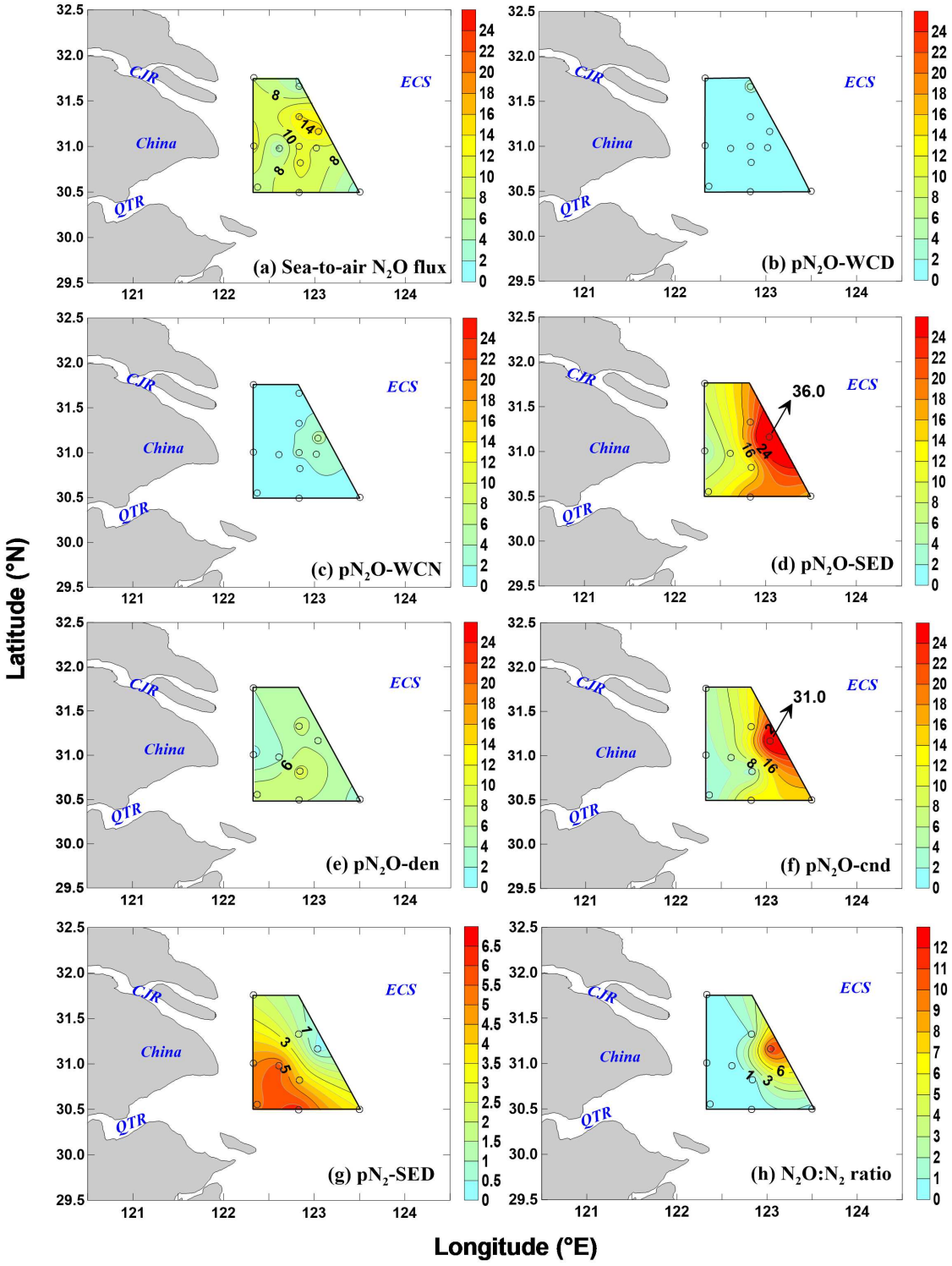

747

748 **Fig. 4.** Spatial distribution of (a) the sea-to-air N_2O flux (μmol m^{-2} day^{-1}), (b) N_2O

749 production rate via water-column denitrification (pN_2O-WCD; μmol m^{-2} day^{-1}), (c) N_2O

750 production rate via water-column nitrification (pN_2O-WCN; μmol m^{-2} day^{-1}), (d) total N_2O

751 production rate via sedimentary processes (pN_2O-SED; μmol m^{-2} day^{-1}), (e) N_2O production

752 rate via sedimentary denitrification (pN_2O-den; μmol m^{-2} day^{-1}), (f) N_2O production rate via

753 sedimentary coupled nitrification-denitrification (pN_2O-cnd; μmol m^{-2} day^{-1}), (g)

754 sedimentary N_2 production rate (pN_2-SED; mmol m^{-2} day^{-1}) and (h) sedimentary N_2O:N_2

755 production ratio (N_2O:N_2 ratio; %) in the hypoxic zone off the CJR estuary.

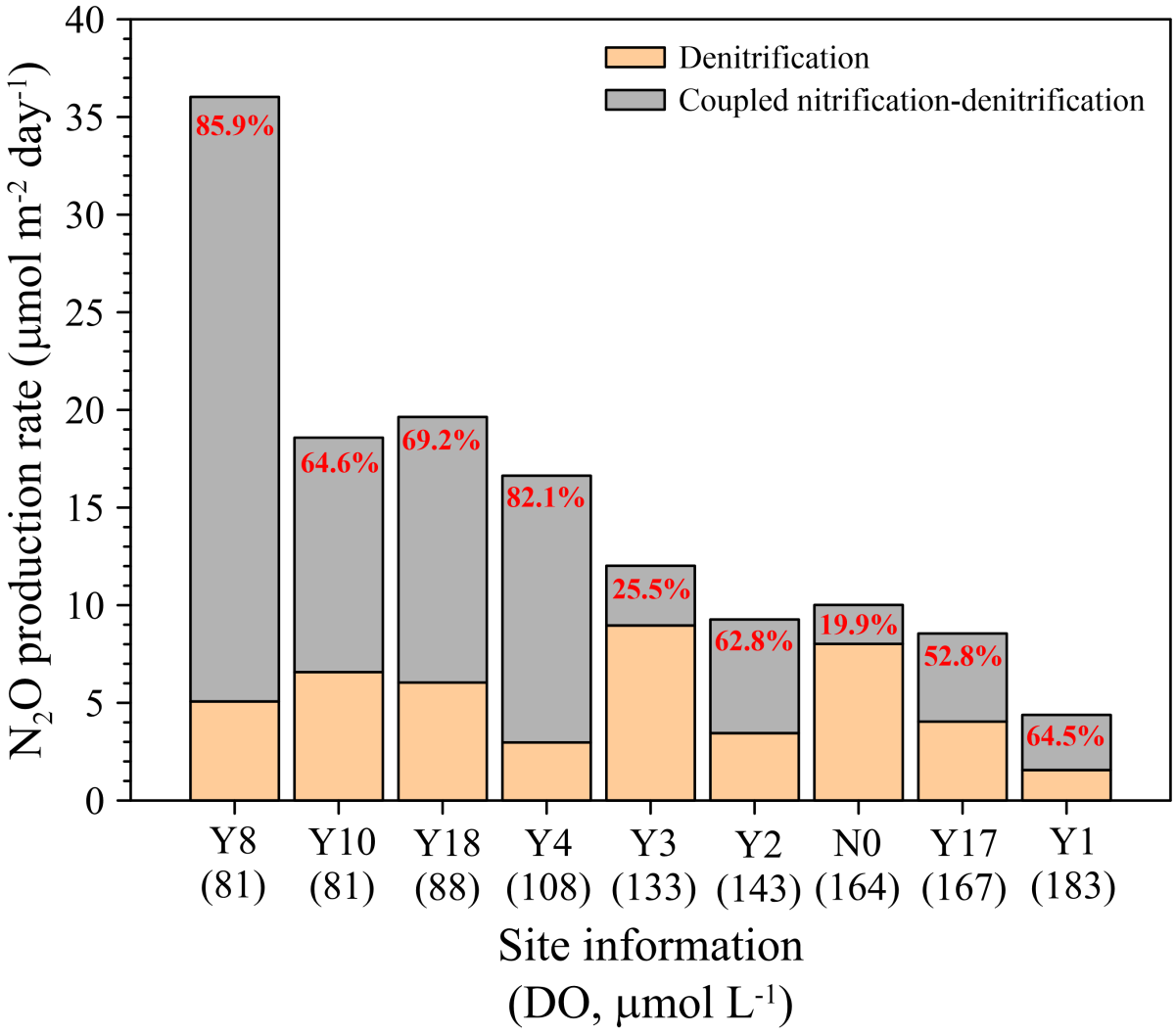

Fig. 5. N_2O production rates via denitrification and coupled nitrification-denitrification (cnd) in the surface sediments in the hypoxic zone off the CJR estuary. Numbers inside the cnd bars denote the relative contribution of cnd to the total sedimentary N_2O production (R_{cnd} in Table 2). Note that we present these datasets along the bottom-water DO gradient (values in units of μmol L^{-1} in parentheses).

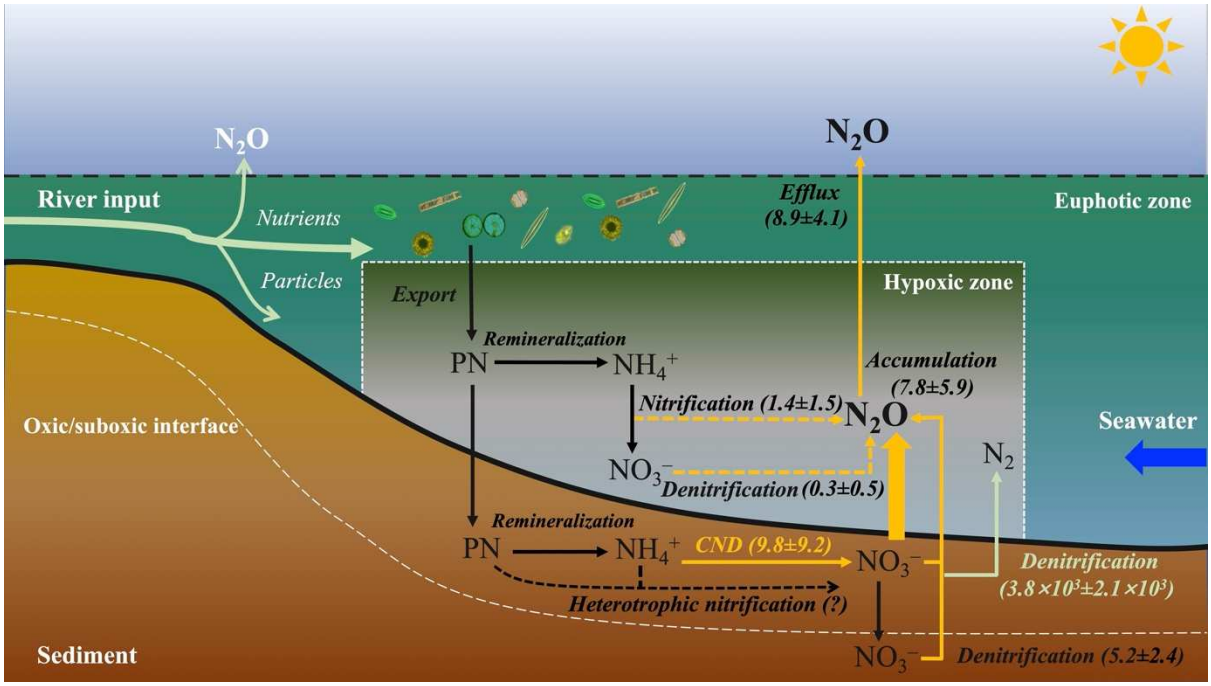

762

763 **Fig. 6.** Conceptual diagram of N_2O production and emission via different pathways in the
764 hypoxic zone off the human-perturbed estuary. CND denotes coupled nitrification-
765 denitrification in sediments. Note that values in units of μmol m^{-2} day^{-1} in parentheses are
766 shown as the N_2O production rates via the water-column and sedimentary processes, the N_2O
767 accumulation rate in the water column, the sea-to-air N_2O flux and sedimentary N_2
768 production rate in the hypoxic zone.